Srere, P. A., & Sumegi, B. (1986) in *Myocardial and Skeletal Muscle Bioenergetics* (Brautbar, N., Ed.) pp 13–25, Plenum Publishing Corp., New York.
Srivastava, D. K., & Bernhard, S. A. (1986) *Science 234*, 1081–1086.
Stryer, L. (1988) *Biochemistry*, 3rd ed., W. H. Freeman & Co., New York.
Sumegi, B., & Alkonyi, I. (1983) *Biochim. Biophys. Acta 749*, 163–171.
Sumegi, B., & Srere, P. A. (1984a) *J. Biol. Chem. 259*, 15040–15045.
Sumegi, B., & Srere, P. A. (1984b) *J. Biol. Chem. 259*, 8748–8752.
Sumegi, B., & Porpaczy, Z. (1989) Structural and Organizational Aspects of Metabolic Regulation, *UCLA Symp. Mol. Cell. Biol., New Ser. 133*, 229–244.
Sumegi, B., Gyocsi, L., & Alkonyi, I. (1980) *Biochim. Biophys. Acta 616*, 158–168.
Tompa, P., Batke, J., Ovadi, J., Srere, P. A., & Welch, G. R. (1987) *J. Biol. Chem. 262*, 6089–6092.
Tyiska, R. L., Williams, J. S., Brent, L. G., Hudson, A. P., Clark, B. J., Robinson, J. B., & Srere, P. A. (1986) in *The Organization of Cell Metabolism* (Welch, G. R., & Clegg, J. S., Eds.) pp 177–189, Plenum Press, New York.
Tzagoloff, A., Akai, A., & Needleman, R. B. (1975) *J. Biol. Chem. 250*, 8228–8235.
Yu, C. A., Yu, L., & King, T. E. (1974) *J. Biol. Chem. 249*, 4905–4910.
Zubay, G. (1988) *Biochemistry*, 2nd ed., Macmillan Publishing Co., New York.

Articles

A Molecular Mechanical Force Field for the Conformational Analysis of Oligosaccharides: Comparison of Theoretical and Crystal Structures of Manα1–3Manβ1–4GlcNAc†

S. W. Homans

Department of Biochemistry, University of Dundee, Dundee DD1 4HN, Scotland, U.K.

Received May 4, 1990; Revised Manuscript Received June 28, 1990

ABSTRACT: A molecular mechanical force field is described for the conformational analysis of oligosaccharides. This force field has been derived by the addition of new parameters to the AMBER force field and is compatible with simulations of proteins. This new parametrization is assessed by comparison of the theoretically predicted conformations of Manα1–3Manβ1–4GlcNAc with the corresponding crystal structure. Molecular dynamics simulation data are presented for this structure both in vacuo and with the explicit inclusion of water molecules. While the former demonstrate significant torsional oscillations about glycosidic linkages at physiological temperature, in the latter these oscillations are highly damped due to the stabilizing influence of a "cage" of solvent–solvent and solvent–solute hydrogen bonds.

The primary tool for the conformational analysis of macromolecules in solution is the ^{1}H NMR nuclear Overhauser effect (NOE) (Noggle & Schirmer, 1971; Neuhaus & Williamson, 1989). By virtue of the inverse sixth power dependence of this parameter upon internuclear distance (r), a highly sensitive conformational "ruler" is available when r is small (<5 Å). However, this function carries with it an inherent penalty when r varies with time, as, for example, in the presence of internal motion. In these cases NOE measurements can suggest a dominant conformer that is completely erroneous since the measured value of the NOE may be heavily weighted in favor of conformers where r is small. Nevertheless, it has been adequately demonstrated that NOE measurements in proteins and nucleic acids can give an average solution structure which compares very favorably with that derived by X-ray diffraction studies (Wuthrich, 1986, and references cited therein). The primary reason for the success of the NOE method lies in the very large number of available distance constraints: when analyzed with distance matrix algorithms in Cartesian or dihedral angle space, the rms atomic deviations at least for the C_α backbone in proteins are sufficiently small for a series of random starting structures that an average solution structure can be defined with confidence (Wuthrich, 1986, and references cited therein). This structure may then be refined by use of energy minimization and molecular dynamics algorithms together with an appropriate molecular mechanical force field (Clore et al., 1986).

In principle, the solution conformations of oligosaccharides can be derived in a manner similar to that for proteins and nucleic acids. However, the above approach has not been adopted for at least two reasons. First, the number of distance constraints available from NOE measurements is very much smaller than in proteins or nucleic acids. Often only one or two NOEs are available across glycosidic linkages, and generally, no NOEs between distance regions of the molecule are observed. Very poor convergence would thus be obtained in distance geometry calculations. Second, a suitable force field for the conformational analysis of oligosaccharides has not been available. Since NOE data in oligosaccharides may not provide sufficient constraints when used alone, the availability

† Financial support provided by the Wellcome Trust.

0006-2960/90/0429-9110$02.50/0

of a full molecular mechanical force field is vital. By use of such a force field, NOE data can be included as pseudo energy terms in energy minimization or molecular dynamics simulations, resulting in a conformation or series of conformations which satisfies both experimental and theoretical criteria.

Here we describe such a force field, which is derived by the addition of new parameters to the AMBER force field (Singh et al., 1986). This new parametrization is assessed by comparison of the crystal structure of Manα1–3Manβ1–4GlcNAc (Warin et al., 1979) with the theoretical minimum energy configuration and average conformation at 300 K both in vacuo and with explicit inclusion of solvent water.

Experimental Procedures

Conventions. The glycosidic torsion angles φ and ψ are analogous to φ_H and ψ_H in IUPAC convention and are defined as H1–C1–O1–CX and C1–O1–CX–HX, respectively, where HX and CX are aglyconic atoms.

Minimizations and Simulations. All calculations were performed with the molecular mechanics package DISCOVER (Biosym Technologies Inc.) interfaced to the AMBER force field. Oligosaccharide structures were created graphically with INSIGHT (Biosym Technologies Inc.), which provides a particularly convenient interface to DISCOVER.

(*a*) *Minimizations.* Energy minimization in vacuo was achieved by use of a quasi-Newton–Raphson algorithm (Fletcher & Powell, 1963) or by use of a steepest-descents algorithm (Fletcher, 1980) in systems containing solvent, until the maximum derivative was less than 0.001 kcal/Å or less than 0.1 kcal/Å in the case of grid searches. The latter were computed in 10° increments about φ and ψ. For certain in vacuo simulations, the effects of solvent were simulated in part by use of a dielectric constant $\epsilon = 80.0$. Minimizations with explicit inclusion of solvent were performed by enclosure of the solute in a box 14 Å × 11 Å × 17 Å containing solvent water molecules and imposition of periodic boundary conditions with an orthogonal *P*1 (identity) space group. A nonbonded cutoff criterion of 10.0 Å was imposed, with a switching distance of 1.5 Å. The nonbonded pair list was updated every 20 iterations.

(*b*) *Molecular Dynamics Simulations.* Molecular dynamics simulations in vacuo and with explicit inclusion of solvent were performed at constant pressure under conditions identical with those described for minimization. In each case the system was equilibrated with a thermal bath at 300 K with a coupling constant of 0.1 ps^{-1}. Simulations were run with a time step of 0.1 fs for 110 ps of real time. Equilibration was monitored empirically by observation of the total energy and was always complete within the first 10 ps. Data analysis was thus performed on the last 100 ps of each simulation by use of in-house-written software. For this purpose, coordinates were stored periodically during the time course of the simulation. The minimum number of such coordinates required to represent adequately the conformational properties of the system during the time course was determined empirically.

(*c*) *Simulated Annealing.* Energy minimization by dynamical simulated annealing was achieved under conditions otherwise identical with those of molecular dynamics simulations, except that the system was equilibrated for 10 ps with a thermal bath at 300 K and thereafter recursively for 1 ps with a thermal bath 10 deg lower in temperature until a final temperature of 10 K was obtained, giving a total simulation time of 30 ps. Following simulation for a further 1 ps at 5 K, the resulting geometry was minimized by use of a steepest-descents algorithm until the maximum derivative was less than 0.001 kcal/Å.

Force Field Development

The form of the AMBER force field (Weiner et al., 1984, 1986), which is the basis of the present work, is as follows:

$$E_{tot} = \underset{\text{bond}}{\sum K_r(r - r_e)^2} + \underset{\text{valence angle}}{\sum K_\theta(\theta - \theta_e)^2} + \underset{\text{torsion angle}}{\sum K_n[1 + \cos(n\varphi - \gamma)]} + \underset{\text{van der Waals}}{\sum\sum \epsilon[-(r^*/r_{ij})^{12} + 2(r^*/r_{ij})^6]} + \underset{\text{electrostatic}}{\sum(q_iq_j/\epsilon r_{ij})} + \underset{\text{hydrogen bond}}{\sum(C_{ij}/r_{ij}^{12} - D_{ij}/r_{ij}^{10})}$$

where the terms have their usual meanings (Weiner et al., 1984).

The AMBER force field in its original form is parametrized on the basis of experimental data for proteins and nucleic acids. Application to oligosaccharides therefore requires reparametrization for structural features characteristic of this molecular type. In the derivation of such parameters, our main concern is in the development of a reliable force field for conformational analysis rather than accurate reproduction of vibrational modes. It is, however, important to give due consideration to the latter, since a good fit between theoretical and experimental vibrational modes lends some confidence that the force field will give meaningful results in molecular dynamics simulations, which may require accuracy of the force field over the whole potential surface, rather than in the region of the global minimum.

Several force-field parametrizations appropriate for carbohydrates have appeared in recent years. Of these, it has been demonstrated by Tvaroska and Perez (1986) that the MM2CARB parametrization of Jeffrey and Taylor (1980) has given the most consistent agreement with experimental data. More recently, Ha et al. (1988a) have described a force field which gives the most accurate reproduction of vibrational modes to date for a monosaccharide (α-D-glucopyranose). Unfortunately, neither of these may be used directly within the framework of the AMBER force field since, on the one hand, the form of the classical "Hamiltonian" in MM2CARB differs fundamentally from that in AMBER and, on the other hand, the force field of Ha et al. contains no torsional terms pertinent to the glycosidic linkage. Although the latter has been applied to maltose (Ha et al., 1988b), the glycosidic linkage was treated the same as ring C–O–C linkages, neglecting the contribution of the exo-anomeric effect (see below).

Since the biologically relevant systems may involve glycoprotein or glycopeptide rather than free oligosaccharide, the addition of parameters relevant to oligosaccharides into AMBER is a highly desirable goal, since then a universal force field is available. The rationale of the present parametrization was thus to combine the parameters for monosaccharides (Ha et al., 1988a) together with more recent ab initio calculations on model compounds pertaining to the glycosidic linkage (Wiberg & Murcko, 1989), in order to generate an AMBER-compatible force field for oligosaccharides which is based upon the most accurate data presently available. In this respect the present approach differs from a recent nonextensive parametrization described by Scarsdale et al. (1988), which involved an empirical parametrization for constrained minimization without application to simulation of molecular dynamics trajectories. The derivation of parameters for the present force field is described sequentially below.

Atom Types. In order to avoid interference with AMBER parameters already in place, new atom types were created specific for oligosaccharides, and these are defined in Table I.

Table I: Force-Field Parameters

atom types (symbol)	mass	type	atom types (symbol)	mass	type
CS	12.0000	sp3 carbon	HY	1.007825	hydroxyl hydrogen
AC	12.0000	α-anomeric carbon	O	15.99491	carbonyl oxygen
BC	12.0000	β-anomeric carbon	OT	15.99491	hydroxyl oxygen
C	12.0000	carbonyl (acetamido) carbon	OH	15.99491	water oxygen
H	1.007825	amido hydrogen	OA	15.99491	α-anomeric oxygen
HT	1.007825	sp3 hydrogen	OB	15.99491	β-anomeric oxygen
AH	1.007825	α-anomeric hydrogen	OE	15.99491	ring oxygen
BH	1.007825	β-anomeric hydrogen	N	14.00307	amido nitrogen
HO	1.007825	water hydrogen			

bond types	K_r	r_e	bond types	K_r	r_e	bond types	K_r	r_e
OH HO	553.0	0.960	AC OA	334.3	1.411	AC OE	296.7	1.427
OT HY	460.5	0.972	BC OB	334.3	1.390	BC OE	296.7	1.427
OA HY	460.5	0.972	CS OA	334.3	1.440	CS N	355.0	1.449
OB HY	460.5	0.972	CS OB	334.3	1.440	H N	434.0	1.010
CS HT	337.3	1.099	CS CS	214.8	1.523	C N	490.0	1.335
AC AH	337.3	1.099	AC CS	214.8	1.523	C O	570.0	1.229
BC BH	337.3	1.099	BC CS	214.8	1.523	C CS	335.0	1.522
AC HT	337.3	1.099	CS OT	334.3	1.411			
BC HT	337.3	1.099	CS OE	296.7	1.427			

angle types	K_θ	θ_e	angle types	K_θ	θ_e	angle types	K_θ	θ_e
HO OH HO	47.0	104.5	BH BC OB	45.9	109.89	BC CS OT	75.7	110.10
CS OT HY	53.6	109.35	HT AC OA	45.9	109.89	CS AC OA	75.7	110.10
AC OA HY	53.6	109.35	HT BC OB	45.9	109.89	CS BC OB	75.7	110.10
BC OB HY	53.6	109.35	HT CS OA	45.9	109.89	CS CS OE	81.0	109.40
CS OT CS	60.0	117.00	HT CS OB	45.9	109.89	CS AC OE	81.0	109.40
AC OA CS	62.0	115.00	HT CS OE	45.2	107.24	CS BC OE	81.0	109.40
BC OB CS	62.0	116.40	HT CS C	35.0	109.50	CS OE CS	90.7	113.80
CS OE AC	90.7	113.80	AH AC OE	45.2	107.24	OE CS OT	92.6	111.55
CS OE BC	90.7	111.90	BH BC OE	45.2	107.24	OE AC OA	92.6	111.55
HT CS HT	33.6	107.85	HT AC OE	45.2	107.24	OE BC OB	92.6	107.40
AH AC HT	33.6	107.85	HT BC OE	45.2	107.24	BC CS N	80.0	109.70
BH BC HT	33.6	107.85	CS CS CS	38.0	110.70	CS CS N	80.0	109.70
HT CS CS	43.0	108.72	CS CS AC	38.0	110.70	HT CS N	38.0	109.50
AH AC CS	43.0	108.72	CS CS BC	38.0	110.70	CS N H	38.0	118.40
BH BC CS	43.0	108.72	CS CS OT	75.7	110.10	CS N C	50.0	121.90
HT CS AC	43.0	108.72	CS CS OA	75.7	110.10	C N H	35.0	119.80
HT CS BC	43.0	108.72	CS CS OB	75.7	110.10	N C O	80.0	122.90
HT CS OT	45.9	109.89	CS C O	80.0	120.40	N C CS	70.0	116.60
AH AC OA	45.9	109.89	AC CS OT	75.7	110.10			

torsion types	K_n	n	γ	torsion types	K_n	n	γ
* CS CS *	1.021	3.0	0.0	CS AC OA CS	0.85	3.0	0.0
* AC CS *	1.021	3.0	0.0	OE AC OA HY	2.15	1.0	300.0
* BC CS *	1.021	3.0	0.0	AH AC OA HY	1.75	2.0	60.0
* CS OT *	0.443	3.0	0.0	CS AC OA HY	0.85	3.0	0.0
* CS OE *	0.928	3.0	0.0	OE BC OB CS	−1.050	1.0	0.0
* AC OE *	0.928	3.0	0.0	BH BC OB CS	1.250	2.0	240.0
* BC OE *	0.928	3.0	0.0	CS BC OB CS	1.400	3.0	0.0
* AC OA *	0.000	0.0	0.0	OE BC OB HY	−1.050	1.0	0.0
* BC OB *	0.000	0.0	0.0	BH BC OB HY	1.250	2.0	240.0
* CS OA *	0.000	0.0	0.0	CS BC OB HY	1.400	3.0	0.0
* CS OB *	0.000	0.0	0.0	HT AC OA CS	0.85	3.0	0.0
* CS N *	0.000	0.0	0.0	HT BC OB CS	1.400	3.0	0.0
* C N *	10.0	2.0	180.0	H N C O	0.650	1.0	0.0
* C CS *	0.0	0.0	0.0		2.500	2.0	180.0
OE AC OA CS	2.15	1.0	300.0	HT CS C O	0.067	3.0	180.0
AH AC OA CS	1.75	2.0	60.0				

van der Waals terms	r^*	ϵ	van der Waals terms	r^*	ϵ	van der Waals terms	r^*	ϵ
CS–	3.60	−0.0903	HT–	2.936	−0.0045	OB–	3.20	−0.1591
AC–	3.60	−0.0903	HO–	2.00	−0.0200	OE–	3.20	−0.1591
BC–	3.60	−0.0903	AH–	2.936	−0.0045	OH–	3.30	−0.1500
C–	3.70	−0.1200	BH–	2.936	−0.0045	O–	3.20	−0.2000
H–	2.00	−0.0200	OT–	3.20	−0.1591	N–	3.50	−0.1600
HY–	1.60	−0.0498	OA–	3.20	−0.1591			

Bond, Angle, and Torsional Parameters. The bond, angle, and torsional parameters for each monosaccharide residue were in general taken directly from Ha et al. (1988a). However, certain parameters required adjustment, and others were added to account for the glycosidic linkage between contiguous monosaccharide residues.

(*a*) *Bonds.* A variety of crystallographic studies and ab initio calculations on di- and trisaccharides indicate that the bond length between the anomeric carbon and the glycosidic oxygen is dependent upon anomeric configuration (Jeffrey et al., 1978). The value of r_e corresponding to this bond in β-glycosidic linkage (bond types BC–OB) was thus adjusted

according to the experimental mean value from crystallographic data (Jeffrey et al., 1978). The corresponding bonds between the glycosidic oxygen and the aglyconic carbon (OA–CS and OB–CS) are rather longer than those in a monosaccharide and were thus adjusted similarly. In each case the force constants were unchanged.

(*b*) *Angles.* The value of θ_e corresponding to the configuration-dependent valence angle between the ring oxygen, anomeric carbon, and glycosidic oxygen in β-configuration monosaccharide residues (OE–BC–OB) was adjusted to the mean value derived from crystallographic data (Jeffrey et al., 1978), and the force constant was unchanged. Similarly, the configuration-dependent valence angle between C5, the ring oxygen, and the anomeric carbon (CS–OE–BC) was adjusted to the mean crystallographic value. Values of θ_e for the glycosidic "bridge" angles between anomeric carbon, glycosidic oxygen, and aglyconic carbon (AC–OA–CS and BC–OB–CS) were determined from experimental mean crystallographic values (Jeffrey et al., 1978). A force constant of 62 kcal/rad^2 for each was derived directly from MM2CARB.

(*c*) *Torsions.* The primary conformational determinants in oligosaccharides are the preferred conformations about the glycosidic angles φ and ψ. It is thus necessary to derive torsional parameters pertaining to these angles (X–AC–OA–X and X–BC–OB–X).

(*i*) φ. Experimental (Lemieux et al., 1979, 1980; Thogersen et al., 1982) and theoretical (Jeffrey et al., 1978; Wolfe et al., 1979) data for glycosidic linkages indicate that the minimum energy value of φ is in the region of +60° in the case of β-D-glycosides and −60° in the case of α-D-glycosides. This phenomenon has been termed the exo-anomeric effect and has its origins in lone pair orbital back-bonding interactions [reviewed by Tvaroska and Bleha (1989)]. On the basis of ab initio molecular orbital calculations on dimethoxymethane (Jeffrey et al., 1978), the influence of the exo-anomeric effect has been included in hard-sphere exo-anomeric effect (HSEA) calculations on oligosaccharides by Lemieux and co-workers (Thogersen et al., 1982). While these calculations have been shown to be of value in simple conformational calculations, the choice of parameters for the exoanomeric effect has been critically assessed by Tvaroska and Perez (1986). In particular, it was shown that the use of a less than optimal basis set (4-31G) combined with rigid geometry in the original calculations (Jeffrey et al., 1978) resulted in a torsional potential with exaggerated barriers to rotation. More recently, an improved series of calculations in dimethoxymethane has been described for the 6-31G* basis set where a relaxed geometry was considered (Wiberg & Murcko, 1989), and the barriers to rotation were indeed significantly lower in this study. In the absence of usable experimental data pertaining to torsional rotation about glycosidic linkages, we have thus parametrized the torsional potential for φ on the basis of these later calculations, using the following strategy. First, a series of molecular mechanical calculations were performed which were analogous to the quantum mechanical calculations of Wiberg and Murcko (1989). Approximate initial geometries for dimethoxymethane were constructed in an appropriate configuration to model the acetal fragment of both α- and β-glycosides and were energy minimized in vacuo by use of the relevant parameters listed in Table I together with appropriate atomic charges (see below). A grid search was performed in 30° increments about the torsion angle corresponding to φ in each case, and the geometries were fully optimized at each point. During each grid search the torsional terms corresponding to φ were set to zero. The difference between the quantum

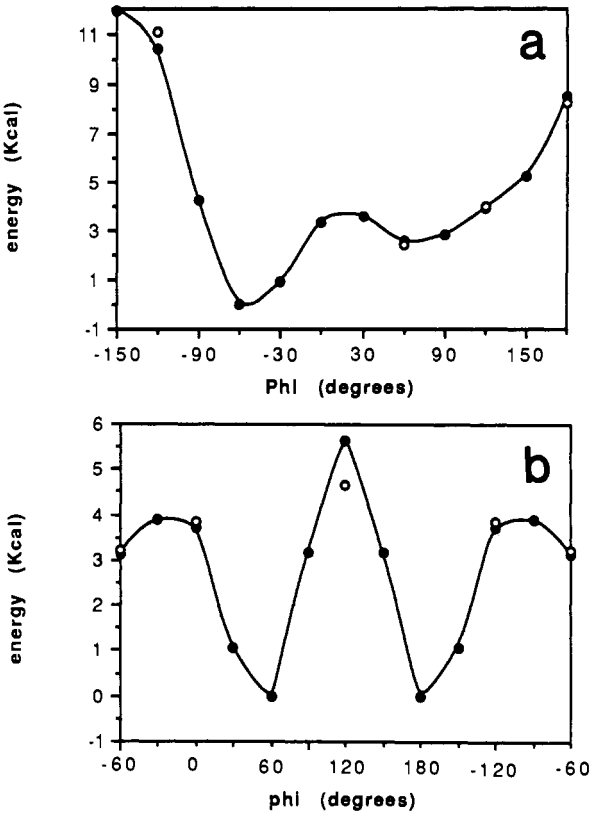

FIGURE 1: Comparison of quantum mechanical [(○) Wiberg & Murcko (1989)] and molecular mechanical [(●) this study] energies for torsional rotation about the angle analogous to φ for two geometries of dimethoxymethane corresponding to (a) α-configuration glycosides and (b) β-configuration glycosides. Note that the molecular mechanical and quantum mechanical energies are coincident at φ = −60° and 0° in (a) and φ = 60° and 180° in (b).

mechanical and molecular mechanical energies, i.e., the error function, was fitted to the AMBER torsional potential in each of the two cases, giving rise to the following expressions:

$$E_{tor}(\alpha\text{-glycosides}) = +2.15[1 + \cos(\theta - 60)] + 1.75[1 + \cos(2\theta - 60)] + 0.85(1 + \cos 3\theta)$$

$$E_{tor}(\beta\text{-glycosides}) = -1.05(1 + \cos\theta) + 1.25(1 + \cos 2\theta) + 1.40(1 + \cos 3\theta)$$

Following this parametrization, each grid search was then recalculated with the relevant torsional constants included, giving molecular mechanical energies for dimethoxymethane which agreed closely with those derived quantum mechanically, as shown in Figure 1. In the fitting of the torsional energies to a relatively simple function, the primary objective was to reproduce faithfully the values at or close to minima at the expense of maxima, on the grounds that precision of the latter are much less important at physiological temperatures. It should be noted that non-zero phase terms were required in the α-anomeric torsional potential to simulate an asymmetric function.

(*ii*) ψ. In HSEA calculations, adequate simulation of the torsional preferences about ψ has been demonstrated without explicit inclusion of torsional terms, which suggests that the values of ψ for both α- and β-D-glycosides appear to be dominated by nonbonded interactions (Bock, 1983). In the present parametrization we have likewise found adequate agreement between simulated and experimental conformational properties without inclusion of explicit torsional terms for ψ. This greatly simplifies force-field development since it obviates the need to derive parameters for every linkage type.

Derivation of Charges. The most difficult aspect of force-field parametrization for oligosaccharides is the deriv-

Table II: Partial Atomic Charges Utilized in the Present Study[a]

atom	charge	atom	charge	atom	charge
C1	0.35	C3	0.15	C5	0.10
H1	0.10	H3	0.10	O5	−0.40
O1	−0.65	O3	−0.65	H5	0.10
OH1	0.40	OH3	0.40	C6	0.05
C2	0.15	C4	0.15	H6A	0.10
H2	0.10	H4	0.10	H6B	0.10
O2	−0.65	O4	−0.65	O6	−0.65
OH2	0.40	OH4	0.40	OH6	0.40

[a] HX refers to the respective carbon-bound hydrogen, and OHX refers to the hydroxyl hydrogen atom. The ring oxygen is designated O5.

ation of charges. In principle, these can be derived either from ab initio or semiempirical quantum mechanical calculations on the relevant structure. However, the values of these charges depend upon the conformation of the molecule. It is therefore most practical to define an average charge for each atom type. This is common practice in the simulation of proteins and nucleic acids (Weiner et al., 1986). In the case of oligosaccharides, the assignment of charges to atom types is however further complicated by branching since the charge state of an aglyconic residue depends upon the number of monosaccharide substituents. In the present parametrization we have utilized the charges derived for monosaccharides by Ha et al. (1988a) (Table II). Charges for substituted monosaccharides were then derived by proportionally modifying those in Table II to maintain neutrality. In practice, this required only a small adjustment for each atom.

van der Waals Terms. All van der Waals terms were taken directly from Ha et al. (1988a) without adjustment.

Hydrogen-Bond Terms. The charges utilized in the parametrization of Ha et al. (1988a) were devised such that hydrogen bonding could be simulated adequately without an explicit hydrogen-bonding term in the "Hamiltonian". Since we have utilized the same charges in the present force field essentially without modification, we likewise set explicit hydrogen-bond terms to zero.

Additional Parameters. All parameters and charges for the acetamido moiety of GlcNAc and for solvent water were derived directly from AMBER.

Results and Discussion

The present parametrization has been assessed by comparison of the conformation of a relevant oligosaccharide for which a good crystal structure has been derived, namely, the trisaccharide Manα1−3Manβ1−4GlcNAc (Warin et al., 1979), with theoretical predictions. First, however, the predicted conformational properties of the disaccharide fragments Manα1−3Man and Manβ1−4GlcNAc were examined independently. It is easier to estimate the minimum energy configurations of these disaccharides independently due to the smaller number of degrees of freedom in comparison with those of the trisaccharide, and these configurations provide a useful check on the worth of the conformationally important torsional parameters.

Manα1−3Man. An approximate starting geometry for Manα1−3Manβ was constructed and energy minimized in vacuo with the appropriate parameters in Table I. In an attempt to determine the values of φ and ψ which correspond to the global minimum energy configuration for this fragment, a grid search was performed by independent variation of each angle in 10° increments. In each case the geometry was fully optimized with a dielectric constant of 80.0 to simulate in part the effects of solvent, giving a total of 1296 energy values in all. These are represented in the form of a contour plot in

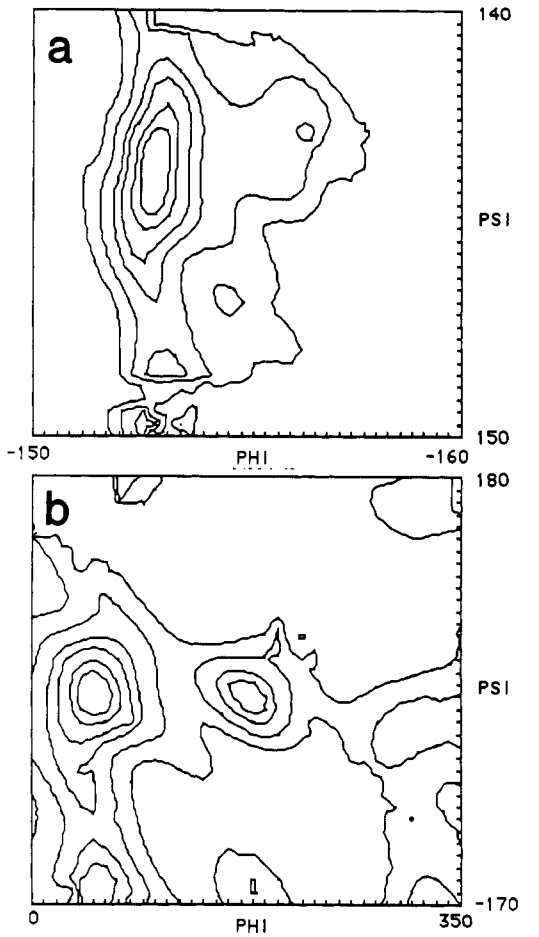

FIGURE 2: Potential surfaces obtained upon rotation about φ and ψ in (a) Manα1−3Manβ and (b) Manβ1−4GlcNAcβ. In each case calculations were performed in vacuo with a dielectric constant = 80.0, and contours are plotted at 0.5, 1.0, 2.0, 3.0, 5.0, and 8.0 kcal above the global minimum.

Figure 2a. The lowest energy conformer was found at φ, ψ = −50°, +20°, and this geometry was fully optimized to generate a global minimum geometry with φ, ψ = −50.5°, +17.8°. It is seen from Figure 2a that several minima are found on the potential surface, and these correspond closely with those derived by Imberty et al. (1989) in the fragment Manα1−3Manα1−OMe. The similarity between the present potential surface and that derived from an independent force-field parametrization (MM2CARB) thus lends confidence in the presently derived torsional parameters for α-glycosides. Notably, both these surfaces predict a much larger fraction of accessible conformational subspace than was predicted in earlier MNDO calculations (Homans et al., 1987), where only a single minimum was found. However, for computational tractability the latter were computed with fixed-ring geometries, and the resulting "tightening" of the potential surface has now been well documented (French, 1989). In an attempt to assess the fraction of conformational subspace defined in Figure 2a which was accessible at physiological temperatures, a molecular dynamics simulation on Manα1−3Manα was performed in vacuo at 300 K with a dielectric constant of 80.0 and was analyzed over a total of 100 ps of real time. The instantaneous values of φ and ψ over this time period are plotted in Figure 3a. It is seen that the value of φ is restricted at around the global minimum at −50°, with occasional excursions to a second minimum around +60°. Similarly, the instantaneous value of ψ is centered around the global minimum at ~0°, with excursions to around 150° and −150° corresponding to additional minima. However, torsional os-

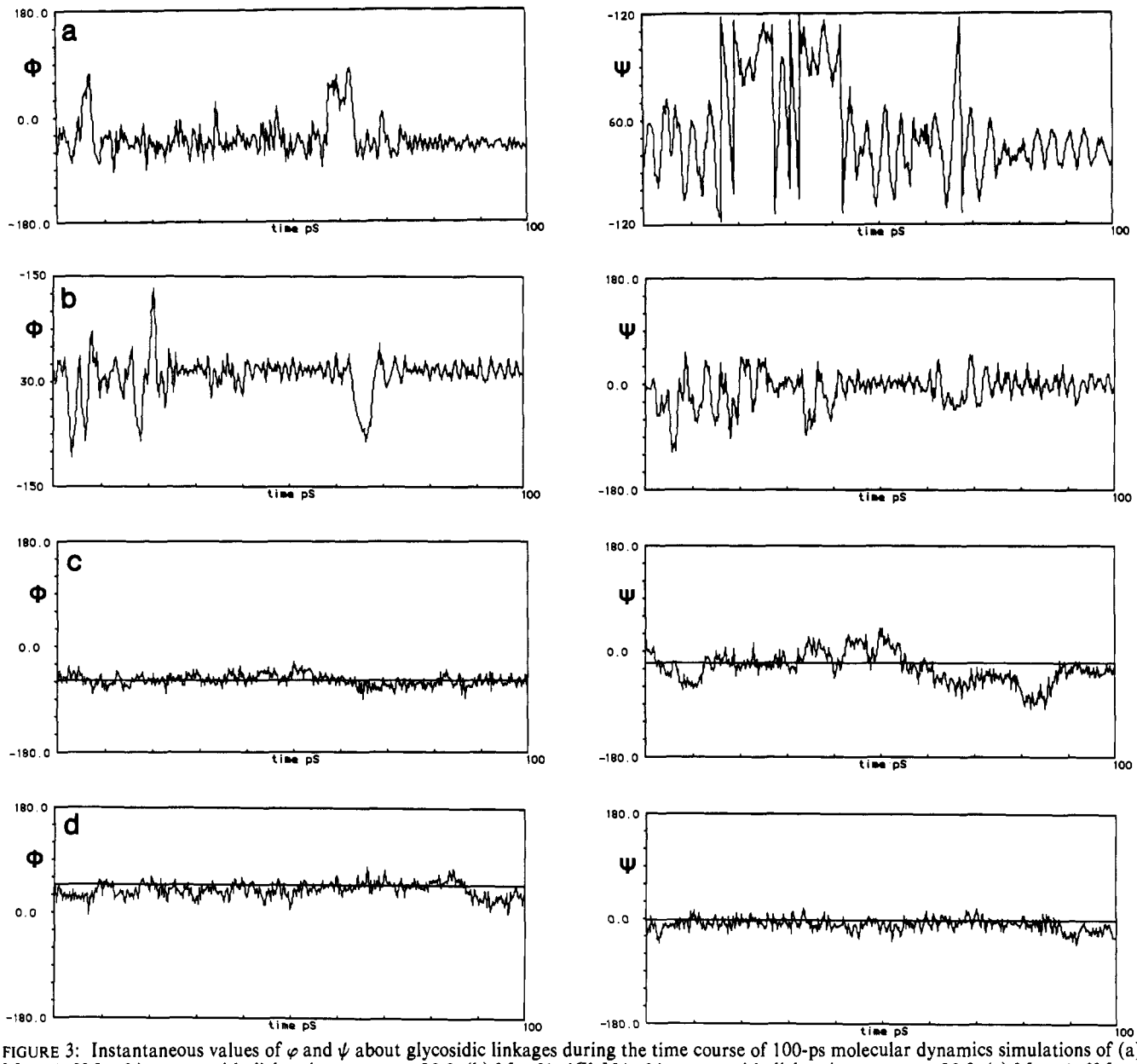

FIGURE 3: Instantaneous values of φ and ψ about glycosidic linkages during the time course of 100-ps molecular dynamics simulations of (a) Manα1-3Manβ in vacuo with dielectric constant = 80.0, (b) Manβ1-4GlcNAcβ in vacuo with dielectric constant = 80.0, (c) Manα1-3Manβ linkage in Manα1-3Manβ1-4GlcNAcβ with explicit inclusion of water, and (d) Manβ1-4GlcNAc linkage in Manα1-3Manβ1-4GlcNAcβ with explicit inculsion of water. In panels c and d, horizontal bars indicate the values of the torsion angles observed in the crystal structure of Manα1-3Manβ1-4GlcNAc (Warin et al., 1979).

cillations about these minima are large, and there is thus significant freedom of motion about ψ under these simulation conditions, as is indeed suggested in qualitative terms from Figure 2a.

Manβ1-4GlcNAc. An entirely analogous series of calculations was performed for Manβ1-4GlcNAcβ, and a contour plot of energies resulting from a grid search about φ and ψ is shown in Figure 2b. The lowest energy conformer was found at $\varphi, \psi = +50°, 0°$, and this geometry was fully optimized to give the global minimum geometry with $\varphi, \psi = +52.0°, 0.52°$, which is consistent with the exo-anomeric effect and thus lends confidence in the derived torsional parameters. The fraction of accessible conformational subspace was again assessed from simulation of molecular dynamics trajectories under conditions identical with those described above for Manα1-3Manα, and the corresponding instantaneous values of φ and ψ are shown in Figure 3b. It is seen that these are both restricted to the region about the global minimum, with occasional excursions to other minima on the potential surface.

Manα1-3Manβ1-4GlcNAc. In order to generate an energy-minimized structure for the trisaccharide, an approximate initial geometry for Manα1-3Manβ1-4GlcNAcβ was generated by combining the global minimum energy geometries of the constituent disaccharide fragments described above. This geometry was then fully optimized in vacuo with a dielectric constant = 80.0 to simulate in part the presence of solvent, thus generating a structure which we term I, with relevant values of φ and ψ as shown in Table III. In order to assess the influence of solvent more exactly, structure I was then immersed in a box of solvent water (see Experimental Procedures) and was again completely optimized (for which the dielectric constant was unity). We refer to this geometry as structure II, and the relevant parameters are also shown in Table III. Although structure II represents a minimum energy structure for the solvated system, it is unlikely to represent the global minimum in view of the very large number of degrees of freedom. These are such that it is practically impossible to estimate the global minimum energy configu-

Table III: Comparison of φ, ψ Values of Glycosidic Linkages for Various Minimized Geometries of Manα1–3Manβ1–4GlcNAc

structure	history	φ, ψ Manα1–3Manα	φ, ψ Manβ1–4GlcNAc	relative energy
I	minimized in vacuo; ϵ = 80.0	−50.7, +18.9	+51.4, 0	0.0
II	minimized in H_2O; ϵ = 1.0	−54.8, +16.0	+43.9, −16.1	−247.93
III	simulated annealing in H_2O; ϵ = 1.0	−48.2, +9.7	+36.8, −19.2	−316.07
IV	average structure at 300 K in H_2O; ϵ = 1.0	−57.9, −28.5	+39.4, −9.8	

ration by use of a grid-search procedure as was utilized above for disaccharide fragments in vacuo. Nevertheless, it is clearly important to estimate the global minimum energy configuration for the solvated system for meaningful comparisons with the crystal structure. We have therefore utilized a different approach to estimate the global minimum energy configuration, namely, simulated annealing. The rationale behind this approach is that if the system is cooled sufficiently slowly from a high initial temperature, then the lowest energy regions of conformational space will be progressively most heavily populated, until at 0 K the system will exist in the global minimum configuration. We have subjected structure II to this procedure as described under Experimental Procedures, giving rise to a third geometry (structure III), which indeed has significantly lower energy than structure II (Table III). Finally, in order to determine accessible regions of conformational space at 300 K, structure III was used as input to a molecular dynamics simulation at 300 K, and the instantaneous values of φ and ψ for each glycosidic linkage are plotted over 100 ps of real time in panels c and d of Figure 3. It is also appropriate to compute an average structure over the time course of the simulation, and we refer to this as structure IV (Table III). A comparison of the four structures indicates that the values of φ and ψ for each glycosidic linkage do not differ greatly. In particular, this suggests that derivation of minimum energy structures of oligosaccharides may be obtained to a good approximation by use of a dielectric constant = 80.0, rather than by explicit inclusion of solvent. However, it will be seen below that explicit inclusion of solvent is important when the motional characteristics of the system are under investigation.

A suitable assessment of the present parametrization is to compare the theoretically predicted geometry with that in the crystal (Warin et al., 1979). For this purpose we have utilized both the "global minimum" energy structure derived by simulated annealing (structure III) and the average structure calculated over the 100-ps molecular dynamics simulation (structure IV). Important conformational angles for each structure are shown in Table IV, together with their rms deviations in the case of structure IV. With notable exceptions described below, it is seen that both structures III and IV are in good agreement with the experimentally derived geometry. However, structure IV is generally in better agreement with experiment, particularly with respect to the values of φ and ψ for each glycosidic linkage. This is to be expected in view of the fact that structure III represents a static structure devoid of the influence of thermal motions.

In the case of the torsion angles C2–C3–C4–C5, C3–C4–C5–O5, and C4–C5–O5–C1 of Manβ, the geometry of both structures III and IV deviates significantly from that of the crystal. This discrepancy almost certainly derives from the fact that the C2, C4, and C6 hydroxyl groups of Manβ in the crystal structure form intermolecular hydrogen bonds, with consequent distortion of ring geometry. Clearly, intermolecular interactions such as these cannot be predicted by simulation of a single molecule and presumably do not exist in solution.

The torsion angles O5–C1–C2–C3 and C1–C2–C3–C4 of GlcNAcβ are significantly different in structure IV compared to those in the crystal. Notably, the rms deviations for these

Table IV: Comparison of Important Conformational Angles (deg) in Structures III and IV (See Text and Table III) with Those in the Crystal Structure of Manα1–3Manβ1–4GlcNAc (Warin et al., 1979)[a]

angle	structure III	structure IV (mean value)	RMS deviation	crystal
Manα1–3				
O5–C1–C2–C3	+58.8	+55.7	6.29	+56.6
C1–C2–C3–C4	−55.5	−54.2	6.67	−54.2
C2–C3–C4–C5	+51.8	+52.5	7.12	+51.8
C3–C4–C5–O5	−51.1	−51.5	7.09	−49.8
C4–C5–O5–C1	+57.8	+56.2	6.72	+54.3
C5–O5–C1–C2	−61.5	−58.6	6.02	−57.0
Manβ1–4				
O5–C1–C2–C3	+58.7	+59.8	6.38	+55.5
C1–C2–C3–C4	−53.4	−57.5	5.95	−55.2
C2–C3–C4–C5	+49.9	+53.7	7.28	+57.9
C3–C4–C5–O5	−50.1	−50.5	7.65	−60.4
C4–C5–O5–C1	+58.6	+54.5	7.04	+64.9
C5–O5–C1–C2	−63.5	−59.3	6.79	−62.6
GlcNAc				
O5–C1–C2–C3	+54.1	+47.9	8.72	+57.5
C1–C2–C3–C4	−49.3	−44.7	8.23	−52.5
C2–C3–C4–C5	+48.9	+48.0	7.67	+50.6
C3–C4–C5–O5	−54.7	−54.7	7.40	−53.5
C4–C5–O5–C1	+63.8	+60.5	7.25	+60.3
C5–O5–C1–C2	−62.1	−56.6	7.71	−62.8
Manα1–3Manα				
φ	−48.2	−57.9	10.20	−57.6
ψ	+9.7	−28.5	26.34	−19.4
C1–O1–C3′	118.3	116.6	3.63	114.1
Manβ1–4GlcNAc				
φ	+36.8	+39.4	13.40	+48.1
ψ	−19.2	−9.8	10.90	−0.6
C1–O1–C4′	120.7	118.8	3.72	114.6

[a] The angles are labeled in obvious notation, with the aglyconic atoms primed where necessary.

angles are significantly larger than all others. This observation, coupled with the fact that the values for the corresponding torsion angles in structure III are in good agreement with the crystal structure, indicates that structure IV is slightly disordered in the region of the anomeric center of GlcNAcβ, suggesting a degree of flexibility in this region of the molecule which, apart from disorder from an admixture of α- and β-anomers, is not observed in the crystal structure. Since structure IV is the result of a "free-solution" simulation, such flexibility is not unexpected in a monosaccharide residue with a free reducing terminus, and this provides a second illustration where solution behavior may differ from that in a crystalline environment.

The mean values of the "bridge" angles in each glycosidic linkage are slightly larger than those in the crystal. While this could potentially be improved by a slight reduction in the value of θ_e, this was not attempted for two reasons. First, it was not clear whether this small discrepancy might again be due to the influence of intermolecular packing forces as described above: significant variation in the values of these angles is apparent in the crystal structures of various carbohydrates, and the "anomalous" low value of both bridge angles was noted in the original work (Warin et al., 1979). Second, the ab initio calculations suggest that the valence angle term corresponding

to the bridge angle is coupled to torsional terms corresponding to the glycosidic linkage. Although small, the question of whether this coupling can be neglected must be deferred pending further assessment of the present force field on a large number of different systems.

It is instructive to compare the instantaneous values of φ and ψ over the 100-ps molecular dynamics simulations for each glycosidic linkage of Manα1–3Manβ1–4GlcNAcβ in vacuo with those computed with explicit inclusion of solvent (Figure 3). It is seen that whereas torsional fluctuations can be large during in vacuo simulations, such fluctuations are highly damped in the presence of solvent and are restricted to values close to those observed in the crystal structure. In order to investigate the mechanism of such damping, a series of 400 geometries over the time course of the simulation with explicit solvent were examined visually. It was apparent that the hydrogen bond observed in the crystal between the C3 hydroxyl of GlcNAc and the ring oxygen of Manβ was present, although transiently broken, during the time course of the simulation, thus stabilizing the Manβ1–4GlcNAc linkage. Furthermore, a transient cagelike network of solute–solvent–solute hydrogen bonds was observed surrounding the structure, which presumably provides an additional stabilizing influence and thus damping of torsional oscillations about glycosidic linkages. In a recent molecular dynamics study of the fragment Manα1–2Manα, damping of torsional oscillations by solvent was similarly observed (Edge et al., 1990). However, the reported potential surface with respect to φ and ψ for the Manα1–2Manα linkage in that study is highly restrained per se. In contrast to our present observations, the potential surface obtained by complete optimization of ring geometry in that study was found to be qualitatively similar to that of an earlier study using rigid-ring geometry (Homans et al., 1987), with a single, deep potential well in each case. In view of the similar conformational properties of Manα1–2Manα and Manα1–3Manα in rigid-geometry calculations (Homans et al., 1987), the reasons for this discrepancy are unclear.

Despite the torsional damping observed in the presence of solvent, significant torsional fluctuations are seen about ψ for the Manα1–3Manα linkage, as evidenced by the instantaneous values plotted in Figure 3c and by the computed rms fluctuation listed in Table IV. In an earlier study (Homans et al., 1987), it was concluded that the Manα1–3Man linkage exists in a single conformation at around $\varphi, \psi = -20°, 50°$ on the basis of MNDO calculations together with a 10-ps molecular dynamics study on Manα1–3Manα. The present work indicates that these earlier studies were inadequate both in the computation of a potential surface using a rigid geometry and in a molecular dynamics simulation of inadequate length. Although the global minimum configuration of the Manα1–3Man linkage predicted in the earlier work is in a low-energy region of the potential surface (Figure 2a), an important additional result of the present work is that the "alternative" configuration of this linkage ($\varphi, \psi = -45°, -15°$) derived by Brisson and Carver (1983b) is also significantly populated at physiological temperatures. By use of a statistical mechanical procedure on the computed potential surface derived from MM2CARB similar to that of Figure 2a and assuming isotropic motion, Imberty et al. (1989) demonstrated that the NOE data of Brisson and Carver (1983a,b) on the Manα1–3Man glycosidic linkage can be interpreted in terms of multiple conformers about this linkage. Similarly, it is tempting to compute theoretical relative NOE values for the same linkage in the present study by use of each discrete geometry generated over the course of the 100-ps molecular dynamics simulation of

Table V: Comparison of Theoretical NOEs Relevant to the Manα1–3Man Glycosidic Linkage Computed over the Time Course of 100-ps Molecular Dynamics Simulation of Manα1–3Manβ1–4GlcNAc in Water with Those Derived Theoretically with MM2CARB by Imberty et al. (1989) and Those Measured Experimentally by Brisson and Carver (1983b)[a]

NOE connectivity	relative NOE		
	present study	MM2CARB	exptl
Man H1–Man H2	1.0	1.0	1.0
Man H1–3Man H3	0.861	0.9	1.0
Man H1–3Man H2	0.044	0.3	0.0
3Man H2–3Man H1	1.0	1.0	1.0
3Man H2–Man H5	0.961	0.8	0.6

[a] NOE connectivities are defined in obvious notation. The estimated error in experimental NOEs is 20% (Brisson & Carver, 1983b).

Table VI: Theoretical NOEs Relevant to the Manα1–3Man Glycosidic Linkage Computed over Four Discrete 25-ps Intervals from the Time Course of 100-ps Molecular Dynamics Simulation of Manα1–3Manβ1–4GlcNAc in Water[a]

NOE connectivity	relative NOE				
	0–25 ps	25–50 ps	50–75 ps	75–100 ps	mean
Man H1–3Man H3	0.786	1.386	0.889	0.383	0.861
Man H1–3Man H2	0.039	0.063	0.0478	0.027	0.044
3Man H2–Man H5	1.187	1.454	0.709	0.494	0.961

[a] NOE connectivities are defined in obvious notation.

Manα1–3Manβ1–4GlcNAc in water. These are shown in Table V and are compared with the NOE values generated experimentally by Brisson and Carver (1983b) and theoretically by Imberty et al (1989). Overall, the theoretical values computed in the present study give, prima facie, rather better agreement with experiment than those obtained by Imberty et al. However, this result may be fortuitous, since the actual NOE values obtained are highly dependent upon the time period of the simulation considered, as shown in Table VI. This result is seen qualitatively in Figure 3c, where the aperiodicity of the torsional fluctuations in ψ is clearly time dependent. This result suggests that it may be necessary to derive theoretical NOE values from molecular dynamics simulations which are computed for a time that is significant with respect to the appropriate NMR time scale. Since the NOE is measured on a time scale on the order of T_1, this suggests that simulations for many tens of milliseconds are necessary, which is clearly impossible with present-day computational resources. In addition, the data of Figure 3 clearly indicate that torsional fluctuations are fast on this time scale, and thus, any formalism for computation of theoretical NOEs will require consideration of the influence of such internal motions. In any event, the fact that theoretical NOE values can be derived which are in reasonable agreement with experimental data for a variety of motional models (Edge et al., 1990; Imberty et al., 1989) including rigid geometry (Brisson & Carver, 1983a,b) suggests that the accuracy of a given force-field parametrization cannot be assessed on this criterion alone.

Conclusions

By use of recently reported ab initio calculations in dimethoxymethane as a model of the glycosidic linkage (Wiberg & Murcko, 1989), we have extended the monosaccharide parameters of Ha et al. (1988a) to generate a molecular mechanical force field for oligosaccharides. The performance of this force field has been assessed primarily by comparison of the crystal structure of Manα1–3Manβ1–4GlcNAc (Warin et al., 1979) with the predicted average conformation at 300 K in solvent water. The agreement between the two structures

is good, suggesting that there are no major flaws in parametrization. However, force fields are continuously evolving entities, and it is anticipated that it will be possible to "fine tune" parameters following extensive comparisons with experimental data from different systems.

An additional aspect of the present work has been a comparison of the accuracy of simulations with explicit inclusion of solvent water with those in vacuo with a dielectric constant of 80.0. While the global minimum geometries of the oligosaccharides are similar in each calculation, the motional characteristics as determined from 100-ps molecular dynamics simulations are completely different. Notably, torsional oscillations about glycosidic linkages are highly damped when solvent is included explicitly, due to the formation of a network of hydrogen bonds around the solute. In earlier studies, it was surmized that intramolecular hydrogen bonding might not significantly influence the conformation of an oligosaccharide due to competition by solvent water (Homans et al., 1986). While an intramolecular hydrogen bond between the C3 hydroxyl of GlcNAc and the ring oxygen of Manβ is indeed seen to be transiently broken during the time course of the molecular dynamics simulation in water, at other times an alternative, stabilizing hydrogen-bond network is seen to result from solute–solvent–solute hydrogen bonds involving a bridging water molecule. Despite the inherent limitations in molecular mechanical simulations of macromolecules, we conclude that inclusion of solvent water, at least in simulations of oligosaccharides, is a necessary criterion for an adequate representation of accessible conformational space.

Acknowledgments

I acknowledge stimulating discussions with Drs. Jeremy Carver and Anne Imberty.

References

Bock, K. (1983) *Pure Appl. Chem. 55*, 605.
Brisson, J.-R., & Carver, J. P. (1983a) *Biochemistry 22*, 3671.
Brisson, J.-R., & Carver, J. P. (1983b) *Biochemistry 22*, 3680.
Clore, G., Brunger, A., Karplus, M., & Gronenborn, A. (1986) *J. Mol. Biol. 191*, 523.
Edge, C. J., Singh, U. C., Bazzo, R., Taylor, G. L., Dwek, R. A., & Rademacher, T. W. (1990) *Biochemistry 29*, 1971.
Fletcher, R. (1980) Unconstrained Optimisation, *Practical Methods of Optimisation*, Vol 1, Wiley and Sons, Chichester, U.K.
Fletcher, R., & Powell, M. J. D. (1963) *Comput. J. 36*, 163.
French, A. (1989) *Carbohydr. Res. 188*, 206.
Ha, S. N., Giammona, A., Field, M., & Brady, J. W. (1988a) *Carbohydr. Res. 180*, 207.
Ha, S. N., Madsen, L. J., & Brady, J. W. (1988b) *Biopolymers 27*, 1927.
Homans, S. W., Dwek, R. A., Boyd, J., Mahmoudian, M., Richards, W. G. & Rademacher, T. W. (1986) *Biochemistry 25*, 6342.
Homans, S. W., Pastore, A., Dwek, R. A., & Rademacher, T. W. (1987) *Biochemistry 26*, 6649.
Imberty, A., Tran, V., & Perez, S. (1989) *J. Comput. Chem. 11*, 205.
Jeffrey, G. A. & Taylor, R. (1980) *J. Comput. Chem. 1*, 99.
Jeffrey, G. A., Pople, J. A., Binkley, J. S., & Vishveshwara, S. (1978) *J. Am. Chem. Soc. 100*, 373.
Lemieux, R. U., Koto, S., & Voisin, D. (1979) *ACS Symp. Ser. 87*, 17.
Lemieux, R. U., Bock, K., Delbaere, L. T., Koto, S., & Rao, V. S. (1980) *Can. J. Chem. 58*, 631.
Neuhaus, D., & Williamson, M. (1989) *The Nuclear Overhauser Effect*, VCH Publishers, Cambridge, U.K.
Noggle, J. H., & Schirmer, R. E. (1971) *The Nuclear Overhauser Effect—Chemical Applications*, Academic Press, New York.
Scarsdale, J. N., Ram, P., Prestegard, J. H., & Yu, R. K. (1988) *J. Comput. Chem. 9*, 133.
Singh, U. C., Weiner, P., Caldwell, J., & Kollman, P. A. (1986) AMBER 3.0, University of California, San Francisco.
Thorgersen, H. Lemieux, R. U., Bock, K., & Meyer, B. (1982) *Can. J. Chem. 60*, 44.
Tvaroska, I., & Perez, S. (1986) *Carbohydr. Res. 149*, 389.
Tvaroska, I., & Bleha, T. (1989) *Adv. Carbohydr. Chem. Biochem. 47*, 45.
Warin, V., Baert, F., Fouret, R., Strecker, G., Spik, G., Fournet, B., & Montreuil, J. (1979) *Carbohydr. Res. 76*, 11.
Weiner, S., Kollman, P. A., Case, D. A., Chandra Singh, U., Ghio, C., Alagona, G., Profeta, S. P., & Weiner, P. (1984) *J. Am. Chem. Soc. 106*, 765.
Weiner, S. J., Kollman, P. A., Nguyen, D. T., & Case, D. A. (1986) *J. Comput. Chem. 7*, 230.
Wiberg, K. B. & Murcko, M. A. (1989) *J. Am. Chem. Soc, 111*, 4821.
Wolfe, S., Whangbo, M.-H., & Mitchell, D. J. (1979) *Carbohydr. Res. 69*, 1.
Wuthrich, K. (1986) *NMR of Proteins and Nucleic Acids*, Wiley, New York.